

All-optical noise spectroscopy of a solid-state spin

Demity Farfurnik,¹ Harjot Singh,¹ Zhouchen Luo,¹ Allan S. Bracker,² Samuel G. Carter,² Robert M. Pettit,^{1,3} and E. Waks¹

¹*Department of Electrical and Computer Engineering,
Institute for Research in Electronics and Applied Physics,
and Joint Quantum Institute, University of Maryland, College Park, MD, USA.*

²*Naval Research Laboratory, Washington, D.C., USA.*

³*Intelligence Community Postdoctoral Research Fellowship Program,
University of Maryland, College Park, MD, USA.*

Noise spectroscopy elucidates the fundamental noise sources in spin systems, which is essential to develop spin qubits with long coherence times for quantum information processing [1], communication [2], and sensing [3]. But noise spectroscopy typically relies on microwave spin control to extract the noise spectrum [4–9], which becomes infeasible when high-frequency noise components are stronger than the available microwave power. Here, we demonstrate an alternative all-optical approach to perform noise spectroscopy. Our approach utilises coherent control using Raman rotations [10, 11] with controlled timings and phases to implement Carr-Purcell-Meiboom-Gill (CPMG) [12] pulse sequences. Analysing the spin dynamics under these sequences extracts the noise spectrum of a dense ensemble of nuclear spins interacting with a quantum dot, which has thus far only been modelled theoretically [13, 14]. While providing large spectral bandwidths of over 100 MHz, our Raman-based approach could serve as an important tool to study spin dynamics and decoherence mechanisms in a broad range of solid-state spin qubits.

Noise spectroscopy using microwave control sequences has shed light on the fundamental noise processes of various spin systems, such as superconducting qubits [4, 5], nitrogen-vacancy centres in diamond [6, 7], and gate-defined quantum dots [8, 9]. In these systems, pulse sequences are used to control the spin dynamics on timescales faster than the environmental noise. The resulting bandwidth of noise spectroscopy is therefore limited by the Rabi frequency of the spin rotation, which must exceed the frequencies of the noise. As such, noise spectroscopy utilizing microwave control becomes challenging in spin systems that exhibit rapid decoherence due to strong interactions with the environment. One example of such a system is InAs/GaAs quantum dots [14–28], which strongly interact with a large nuclear background [14–17, 29, 30], and exhibit low electron g-factor of ~ 0.4 [18]. Due to this low g-factor, deterministically addressing single quantum dots using microwave fields requires the development of advanced circuitry, which becomes even more challenging for quantum dots embedded in optical cavities used for photonic applications. As a result, experimentally realised microwave control of

the quantum dot spin is typically orders of magnitude weaker [19] than required (\sim tens of MHz [13, 14]) for noise spectroscopy. Thus, such noise spectroscopy requires an alternative approach for controlling the quantum dot spin. Traditionally, all-optical techniques for controlling the quantum dot spin utilise ultrafast pulsed lasers [14, 15]. In these techniques, however, the timing and phases of the rotation pulse are dictated by the repetition rate of the laser and cannot be fully controlled for the implementation of pulse sequences required for noise spectroscopy. While a more precise optical control of the quantum dot spin control has been recently demonstrated [10], noise spectroscopy of the quantum dot environment has yet to be realised.

In this letter, we realise all-optical noise spectroscopy on a single spin confined in a quantum dot using Raman-based spin control. By fully controlling the times, amplitudes, and phases of spin rotation pulses, we implement CPMG control sequences to probe the spin dynamics associated with the noise. We analyse the resulting spin dynamics to extract the noise spectra with bandwidths of over 100 MHz. These high bandwidths enable the measurement of spectra under external magnetic fields up to 2 T, which feature frequencies that significantly increase with the magnetic field due to the spread of Larmor frequencies of the background nuclei. The extracted noise spectra verify a theoretical model that considers two spectral components associated with the strained environment of quantum dots and lead. In addition, the extracted noise frequencies and amplitudes can be used to provide insights into the spin dynamics resulting from the application of any coherent control, including dynamical decoupling sequences for the extension of spin coherence times. As such, our all-optical approach for noise spectroscopy enables the evaluation of quantum dots and other optically active spin systems for quantum information processing, communication, and sensing.

The spin we use to demonstrate all-optical spectroscopy is a negatively charged quantum dot. Under an external magnetic field applied in perpendicular to the sample growth direction (Voigt geometry), the electronic structure of these dots consists of an electron ground-state spin qubit ($\{|\uparrow\rangle, |\downarrow\rangle\}$) and two optically excited trion states ($\{|\uparrow\downarrow, \uparrow\rangle, |\uparrow\downarrow, \downarrow\rangle\}$) [18], as illustrated in Fig. 1a. Spontaneous decay from the excited states leads to fluorescence emission of single photons (exemplified

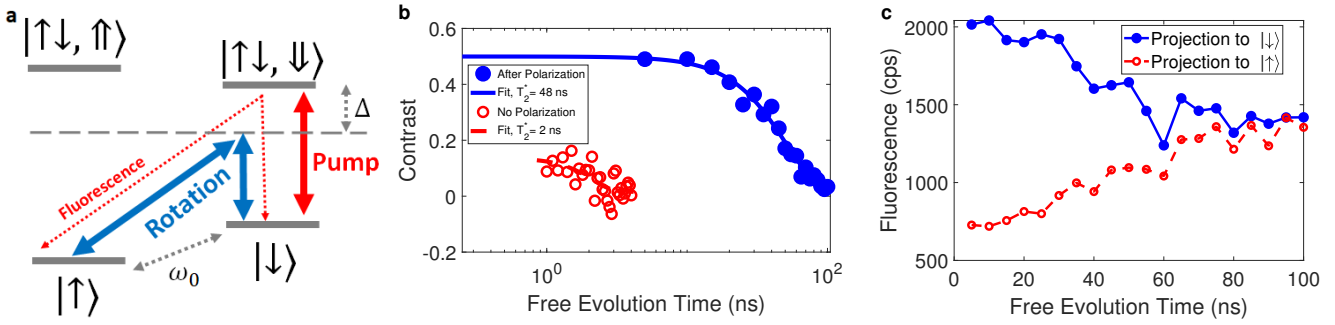


Fig. 1 | Raman spin control of a quantum dot to introduce pulse sequences for noise spectroscopy. **a**, The energy-level diagram of a negatively charged quantum dot under an external magnetic field in the Voigt geometry, including the optical pumping (red, solid arrows) and Raman rotation (blue, solid arrow) transitions used for noise spectroscopy, as well as the optical decay transitions from the excited state (red, dashed arrow). Fluorescence collected from the diagonal optical decay transition indicates the quantum dot spin state. **b**, The Ramsey experiment used to characterise our preliminary polarisation of the nuclear ensemble. The resulting spin dynamics without (red, dashed line) and with (blue, solid line) polarisation of the nuclear spin environment at an external field of $B = 2.4$ T shows the electron spin coherence time can be extended from $T_2^* \approx 2$ ns (red dashed line) to $T_2^* \approx 4$ ns (blue solid line). **c**, Raw data obtained by projecting the final spin state to the different electron ground states after implementation of the 4 μ s nuclear polarisation and Ramsey sequence. Normalizing both curves with respect to each other resulted in the Blue solid line in **b**.

for $|\uparrow\downarrow, \downarrow\downarrow\rangle$ by dotted arrows in Fig. 1a) with high efficiency and indistinguishability [20–23], positioning quantum dots as promising platforms for quantum communication and networking [24–28]. The quantum dot spin is susceptible to magnetic noise governed by the ensemble of indium and arsenic nuclear spins, also known as the Overhauser field [13–16], which we experimentally characterise here using an all-optical control.

To perform all-optical coherent control of the quantum dot spin, we utilise detuned Raman excitations [10]. This Raman approach involves the two-photon resonant excitations of the quantum dot ground states (blue solid arrows in Fig. 1a) that introduces spin rotations with a Rabi frequency of ≈ 150 MHz. A modulation of the rotation laser introduced by an arbitrary waveform generator allows us to generate rotation pulses in the rotating frame of the quantum dot spin with precise timings, amplitudes, and phases (see Methods). To ensure that spin dephasing is minimal during the application of the rotation pulses, we also leverage these precise control capabilities to polarise the bath of indium and arsenic nuclear spins prior to the application of any pulse sequence [11] (see Methods).

After such polarisation of the nuclear spins, we measure the quantum dot coherence using Ramsey spectroscopy, resulting in a decay function with a timescale T_2^* (Fig. 1b-c; see Methods). The nuclear bath polarisation increases the inhomogeneous coherence time from $T_2^* \approx 2$ ns (red dashed line in Fig. 1b) to $T_2^* \approx 48$ ns (blue solid line in Fig. 1b), consistent with previous Ramsey measurements [11]. The spin dephasing time is therefore over an order of magnitude longer than the π -pulses used in CPMG sequences implemented here.

The CPMG sequences [12] implemented for noise spectroscopy are illustrated in Fig. 2a. After a preliminary 4

μ s long step of nuclear spin polarisation, we initialise the spin in the state $\frac{|\uparrow\rangle+|\downarrow\rangle}{\sqrt{2}}$ using an optical pumping pulse followed by a $\frac{\pi}{2}$ -rotation pulse (see Methods). Then, we apply $n \geq 1$ equally spaced π -pulses that modify the spin dynamics. After the application of a second $\frac{\pi}{2}$ -pulse, a final optical pumping pulse induces a fluorescence signal that indicates the final spin state. Collecting the fluorescence while increasing spin interrogation time (i.e., the time between the $\frac{\pi}{2}$ -pulses), t , results in a decay of spin coherence represented by a coherence function, $C(t)$. Such a temporal sweep of the spin interrogation time, uniquely enabled by the precise timing of our Raman pulses, allows us to analyse the spin dynamics for noise spectroscopy.

We first apply the simplest form of CPMG sequence, namely the Hahn-echo experiment consisting of a single π -pulse (Fig. 2b). Consistent with previous Hahn-echo measurements on quantum dots [14–16], the decay timescale of the spin dynamics (i.e. the coherence time) increases as a function of the external magnetic field, B , up to $T_2 \approx 1$ μ s (blue, solid line in Fig. 2b). This increase can be associated with Zeeman terms of the indium and arsenic nuclei dominating over the sources of decoherence at high magnetic fields (Supplementary Note 1). Furthermore, the spin dynamics under any magnetic field exhibit a two-stage decoherence behaviour that consists of a fast drop of the signal contrast, followed by a second decay (starting at $t \approx 100$ ns). This behaviour is analogous to the previously observed Hahn-echo spin dynamics of InGaAs quantum dots [14, 16]. Intuitively, the two stages of decoherence suggest that separate spectral components of the noise affect the spin dynamics at separate timescales. Simulation results (Fig. 2c), which consider such separate noise components associated with the strained nuclear environment of the quantum dot

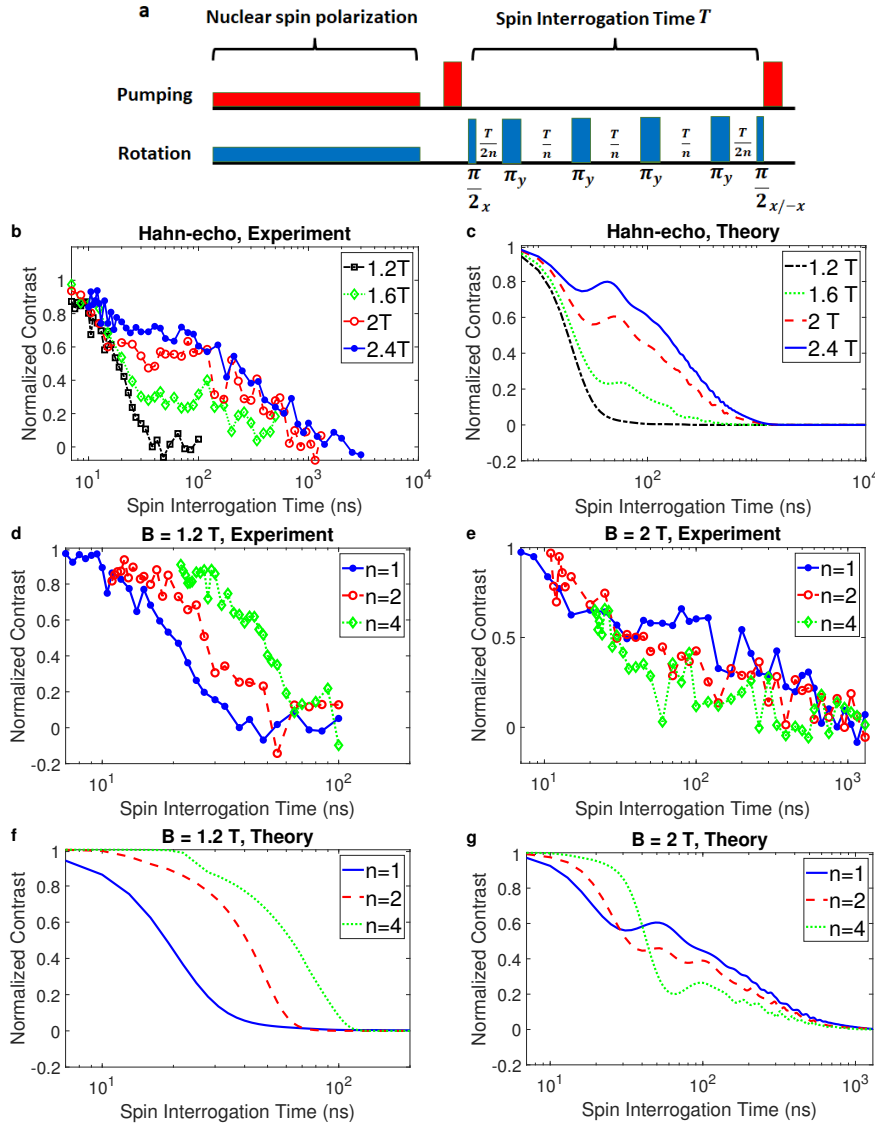


Fig. 2 | Coherence functions obtained from the application of CPMG sequences on a quantum dot spin. **a**, Representative scheme of a CPMG sequence, with $n = 4$ pulses and total interrogation time t , performed after 4 μ s of nuclear polarisation. The phase of the π -pulses is perpendicular to the phase of the $\frac{\pi}{2}$ -pulses. The phase of the last pulse is alternated between 0° and 180° for normalisation purposes. The pumping and rotation amplitudes for nuclear polarisation (illustrated by the heights of the pulses) are weaker than those used for spin interrogation. **b-g**, Normalised experimental and simulated coherence functions of a quantum dot spin under the application of CPMG sequences with n pulses. The experimental results (**b**) and simulations (**c**) of the Hahn-echo sequence ($n = 1$) at different magnetic fields, B . The experimental results (**d**, **e**) and simulations (**f**, **g**) of multi-pulse CPMG sequences at $B = 1.2$ T and $B = 2$ T, respectively.

[13, 14] (Supplementary Note 1), agree with the experimental results, thereby confirming this intuitive assessment. However, to experimentally extract these spectral components requires the application of CPMG sequences with increasing numbers of pulses.

We study the spin dynamics with increasing numbers of π -pulses for different external magnetic fields. For $B = 1.2$ T, the measured spin coherence times (Fig. 2d) clearly increase with n as the decay timescale of the coherence function becomes longer. For $B = 2$ T, however,

the two-stage spin decoherence profile exhibits a more complicated behaviour (Fig. 2e) as a function of n . Our simulations (shown in Fig. 2f and Fig. 2g for $B = 1.2$ T and $B = 2$ T, respectively) considering two spectral components of the Overhauser field [13, 14] agree with the experimental behaviour. However, to understand the impact of adding π -pulses to the CPMG sequence on the spin dynamics requires a comparison between the rate of application of these pulses with the frequencies of the noise spectra [4, 6–9, 31–33]. We can experimentally ex-

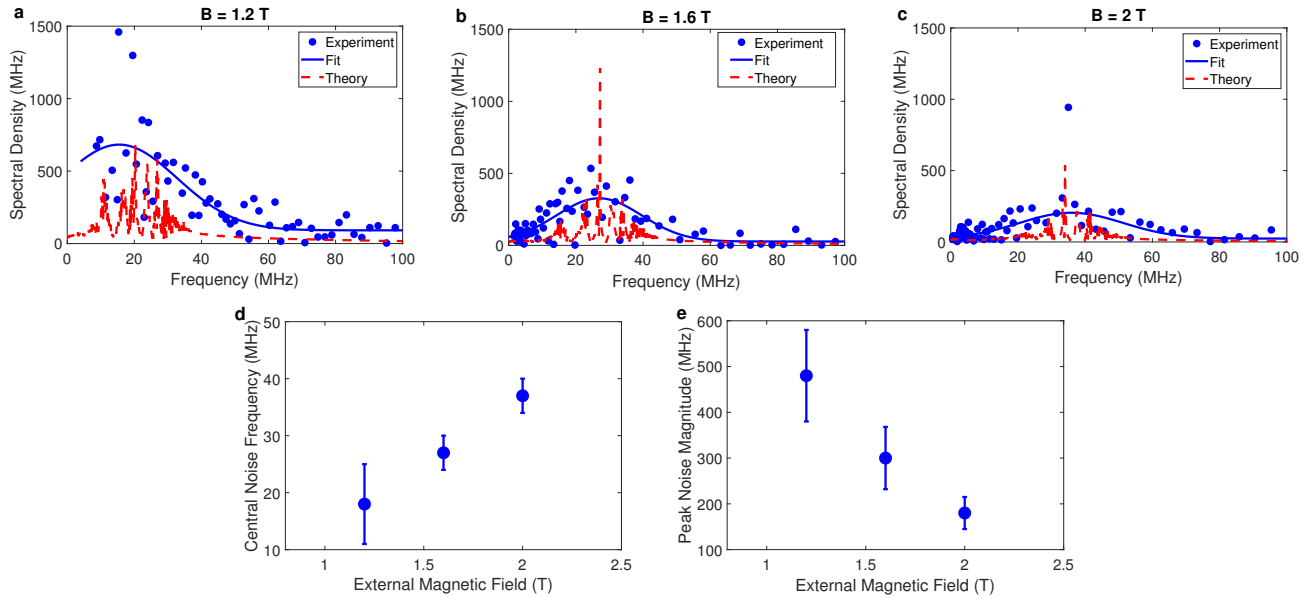


Fig. 3 | Noise spectroscopy of the quantum dot environment. **a-c**, Noise spectroscopy of the nuclear spin ensemble interacting with a quantum dot, derived from spectral decomposition of CPMG experiments with $n = 1, 2, 4$ and 8 pulses at varying magnetic fields of $B = 1.2$ T (a), $B = 1.6$ T (b), and $B = 2$ T (c). The blue dots represent experimental results, the blue solid lines represent fitting of these results to Gaussian functions, and the red dashed lines represent simulations considering $30,000$ nuclear spins. **d**, The central frequency and **e**, magnitude at the central frequency of the noise spectral density as a function of the magnetic field, extracted from the Gaussian fitting in **a-c**, with error bars obtained from the least-square fitting algorithm.

tract these noise frequencies by the numerical analysis of the measured coherence functions.

To perform this analysis, we treat the Overhauser field as a semi-classical noise source [6, 14] with a spectral density $S(\omega)$. In this treatment, the spin dynamics under the application of a pulse sequence satisfy [32, 33]

$$\chi(t) = \int_0^\infty \frac{S(\omega)F(\omega t)}{\pi\omega^2} d\omega \quad (1)$$

where $F(\omega)$ is the filter function that represents a control sequence in the frequency domain, and $\chi(t) = -\ln[C(t)]$. We use the measured coherence functions, $C(t)$, and known CPMG filter functions, $F(\omega)$ [32], for $n = 1, 2, 4$ and 8 , to spectrally deconvolve equation (1) and extract the noise spectra [7] (see full algorithm in Supplementary Note 2).

The extracted spectral densities, plotted for external magnetic fields between 1.2 T and 2 T (data points in Fig. 3a-c), display a broad range of frequencies. The high spectral bandwidth of noise spectroscopy provided by the Raman approach enables the identification of such frequencies up to 100 MHz. To characterise the behaviour of the noise as a function of the magnetic field, we fit the extracted spectra to Gaussian functions (blue, solid lines in Fig. 3a-c). The central frequency of the noise (centre of the Gaussian fit) increases with the magnetic field up to 38 MHz at $B = 2$ T (Fig. 3d), consistent with the increase of the nuclear Larmor frequencies. Meanwhile, the amplitude of the noise (at the central frequency) de-

creases with the magnetic field (Fig. 3e) as nuclear Zeeman interactions dominate over sources of decoherence.

The extracted noise spectra verify the theoretical model we use for the Overhauser field [13, 14]. Simulated spectra considering this model (red, solid lines in Fig. 3a-c) represent the hyperfine coupling of the quantum dot spin to nuclear spins experiencing quadrupolar coupling to strain fields. The amplitudes of the simulated spectra consistently fit the experimentally extracted amplitudes (Fig. 3e) and indicate that the quantum dot spin interacts with $30,000$ nuclei (Supplementary Note 1), in agreement with common predictions [14]. The theoretical noise spectra consist of two separate terms, perpendicular and parallel to the direction of the external magnetic field [13, 14]. The noise component perpendicular to the external field monotonically decreases with the frequency and qualitatively fits the experimentally extracted noise floor (baselines of the Gaussian fits in Fig. a-c). This noise component dominates at low frequencies (< 10 MHz, Supplementary Note 1), thereby leading to the spin dynamics at long timescales (> 100 ns) depicted in Fig. 2b-g. Since the application rate of π -pulses in our CPMG sequences is faster than these low frequencies, increasing the number of pulses slows down the decay of the spin dynamics at long timescales. For example, under an external field of 2 T (Fig. 2e), the decay of the spin dynamics at $t > 100$ ns is slower for $n = 4$ (green, dotted line) than for $n = 1$ (blue, solid line). Meanwhile, the high frequency noise that dictates the spin dynam-

ics at short timescale arises in parallel to the direction of the external field [13, 14]. This term is stronger than the perpendicular noise term and consists of peaks corresponding to the nuclear Larmor frequencies broadened by the environmental strain field (Supplementary Note 1). These broad features lead to the observed contrast drop of the spin dynamics [33] depicted in Fig. 2b-g at short timescales. The application rate of π -pulses in our CPMG sequences under a magnetic field of 2 T is slower than these high frequency components of the noise. As a result, the decay of the spin dynamics at timescales shorter than 100 ns does not improve by increasing the number of pulses (Fig. 2e). Such a challenge in mitigating the high frequency noise has so far limited observed quantum dot spin coherence times to a few microseconds [14–16]. By plugging the obtained noise spectra back to equation (1), we learn that these coherence times could be extended beyond 10 μ s with dynamical decoupling sequences utilizing hundreds of π -pulses.

However, here we were able to apply just eight π -pulses due to two mechanisms of spin relaxation. First, the natural spin relaxation of the quantum dot in our sample, $T_1 \approx 1 \mu\text{s}$, did not allow us to observe expected spin dynamics under multi-pulse sequences beyond microsecond timescales. This relaxation time could be extended up to milliseconds by modifying the tunnel barrier of the sample [34]. Second, increasing the number of CPMG pulses in our measurements resulted in a dramatic contrast drop of the collected fluorescence as a function of n [10] (Sup-

plementary Note 3). This contrast drop is related to electron tunnelling due to the increase of the laser power associated with the addition of the pulses. Such electron tunnelling could be mitigated by enhancing the coupling of the quantum dot to the rotation laser by fabricating photonic structures on the sample, enabling spin rotations using lower laser power. These low power rotations could then enable multi-pulse sequences prolonging spin coherence times. Furthermore, the application of hundreds of pulses could enable the realisation of advanced pulse sequences for high resolution quantum sensing (e.g., DYSCO [7] sequences), and for the preservation of arbitrary spin states (e.g., XY8-based sequences [31]) for quantum information processing.

To conclude, we introduce an all-optical approach for noise spectroscopy and implement it to study the environment of InAs quantum dots, for which the application of microwave control is challenging. Leveraging the high Rabi frequencies and precise control capabilities of the Raman approach provides spectral bandwidths ($> 100 \text{ MHz}$) that enable the identification of high frequency noise spectra. Our method can be adopted to any solid-state system incorporating optically active spin qubits. The extracted noise spectra can be used to predict spin dynamics under the application of various control sequences and to understand the behaviour of spin coherence, thereby evaluating the potential of spin qubits for the applications of quantum sensing, communication, and information processing.

[1] D. P. DiVincenzo, “The physical implementation of quantum computation,” *Fortschr. Phys.* **48**, 771–783 (2000).

[2] N. Gisin and R. Thew, “Quantum communication,” *Nat. Photonics.* **1**, 165–171 (2007).

[3] C. L. Degen, F. Reinhard, and P. Cappellaro, “Quantum sensing,” *Rev. Mod. Phys.* **89**, 035002 (2017).

[4] J. Bylander *et al.*, “Noise spectroscopy through dynamical decoupling with a superconducting flux qubit,” *Nat. Phys.* **7**, 565–570 (2011).

[5] Y. Sung *et al.*, “Multi-level quantum noise spectroscopy.” *Nat. Commun.* **12**, 967 (2021).

[6] N Bar-Gill *et al.*, “Suppression of spin-bath dynamics for improved coherence of multi-spin-qubit systems.” *Nat. Commun.* **3**, 858 (2012).

[7] Y. Romach *et al.*, “Measuring Environmental Quantum Noise Exhibiting a Nonmonotonic Spectral Shape,” *Phys. Rev. Applied* **11**, 014064 (2019).

[8] F. K. Malinowski *et al.*, “Notch filtering the nuclear environment of a spin qubit.” *Nat. Nanotechnol.* **12**, 16–20 (2017).

[9] K. Chan *et al.*, “Assessment of a silicon quantum dot spin qubit environment via noise spectroscopy.” *Phys. Rev. Applied* **10**, 044017 (2018).

[10] J. H. Bodey *et al.*, “Optical spin locking of a solid-state qubit,” *npj Quantum Inf.* **5**, 95 (2019).

[11] D. A. Gangloff *et al.*, “Quantum interface of an electron and a nuclear ensemble.” *Science* **364**, 62–66 (2019).

[12] S. Meiboom and D. Gill, “Modified spin-echo method for measuring nuclear relaxation times,” *Rev. Sci. Instrum.* **29**, 688–691 (1958).

[13] C. Bulutay, “Quadrupolar spectra of nuclear spins in strained inxgal-xas quantum dots.” *Phys. Rev. B* **85**, 115313 (2012).

[14] R. Stockill *et al.*, “Quantum dot spin coherence governed by a strained nuclear environment,” *Nat. Commun.* **7**, 12745 (2016).

[15] D. Press *et al.*, “Ultrafast optical spin echo in a single quantum dot.” *Nat. Photonics.* **4**, 367–370 (2010).

[16] A. Bechtold *et al.*, “Three-stage decoherence dynamics of an electron spin qubit in an optically active quantum dot,” *Nat. Phys.* **11**, 1005–1008 (2015).

[17] A. V. Kuhlmann *et al.*, “Charge noise and spin noise in a semiconductor quantum device.” *Nat. Phys.* **9**, 570–575 (2013).

[18] M. Bayer *et al.*, “Fine structure of nuclear and charged excitons in self-assembled in(ga)as/(al)gaas quantum dots.” *Phys. Rev. B* **65**, 195315 (2002).

[19] M. Kroner *et al.*, “Optical detection of single-electron spin resonance in a quantum dot,” *Phys. Rev. Lett.* **100**, 156803 (2008).

[20] X. Ding *et al.*, “On-demand single photons with high extraction efficiency and near-unity indistinguishability from a resonantly driven quantum dot in a micropillar,” *Phys. Rev. Lett.* **116**, 020401 (2016).

[21] N. Somaschi *et al.*, “Near-optimal single-photon sources in the solid state,” *Nat. Photonics.* **10**, 340 (2016).

- [22] E. Schöll *et al.*, “Resonance fluorescence of gaas quantum dots with near-unity photon indistinguishability,” *Nano Lett.* **19**, 2404–2410 (2019).
- [23] N. Tomm *et al.*, “A bright and fast source of coherence single photons.” *Nat. Nanotechnol.* **16**, 399–403 (2021).
- [24] W. B. Gao, P. Fallahi, E. Togan, J. Miguel-Sánchez, and A. Imamoglu, “Observation of entanglement between a quantum dot spin and a single photon.” *Nature* **491**, 426–430 (2012).
- [25] P. Lodahl, “Quantum-dot based photonic quantum networks.” *Quantum. Sci. Technol.* **3**, 013001 (2018).
- [26] M. H. Appel *et al.*, “Coherent spin-photon interface with waveguide induced cycling transitions.” *Phys. Rev. Lett.* **126**, 013602 (2021).
- [27] S. Sun, H. Kim, Z. Luo, G. H. Solomon, and E. Waks, “A single-photon switch and transistor enabled by a solid-state quantum memory,” *Science* **361**.
- [28] “A spin-photon interface using charge-tunable quantum dots strongly coupled to a cavity,” .
- [29] E. A. Chekhovich *et al.*, “Nuclear spin effects in semiconductor quantum dots.” *Nat. Mater.* **12**, 494–504 (2013).
- [30] G. Wüst *et al.*, “Role of the electron spin in determining the coherence of the nuclear spins in a quantum dot.” *Nat. Nanotechnol.* **11**, 885–889 (2016).
- [31] D. Farfurnik *et al.*, “Optimizing a dynamical decoupling protocol for solid-state electronic spin ensembles in diamond,” *Phys. Rev. B* **92**, 060301(R) (2015).
- [32] L. Cywinski, R. M. Lutchyn, C. P. Nave, and S. Das Sarma, “How to enhance dephasing time in superconducting qubits,” *Phys. Rev. B* **77**, 174509 (2008).
- [33] Rogerio de Sousa, “Electron spin as a spectrometer of nuclear-spin noise and other fluctuations,” in *Electron Spin Resonance and Related Phenomena in Low-Dimensional Structures*, Topics in Applied Physics, Vol. 115 (Springer, Berlin, 2009) pp. 183–220.
- [34] G. Gillard *et al.*, “Fundamental limits of electron and nuclear spin qubit lifetimes in an isolated self-assembled quantum dot.” *npj Quantum Inf.* **7**, 43 (2021).

METHODS

Sample Growth. We use a sample grown by molecular beam epitaxy consisting of InAs quantum dots embedded in a GaAs p-i-n-i-n diode. The diode is an optical cavity, sandwiched between distributed Bragg reflectors, consisting of 10 and 4 periods of GaAs/AlAs layers below and above the cavity, respectively. The diode enabled the charging of the quantum dot with a single electron by the application of a voltage bias. The cavity directed the fluorescence emitted from the dot toward our collection port, thereby enhancing the measured signals.

Experimental Setup. The sample was mounted in a low vibration He exchange gas cryostation with a base temperature of ~ 4.3 K (attocube attoDRY1000). A superconducting coil provided magnetic fields of 1–3 T perpendicular to the growth direction of the quantum dot (Voigt geometry), under which we performed noise spectroscopy of the quantum dot environment. Note, we observed agreement between the theoretical and experimental data (Fig. 2-3) considering magnetic fields that

were 1.25 times weaker than those set on the magnet controller. We attribute this factor to attenuations in the cryostation and misalignment of the sample from the main axis of the magnet.

Two circularly polarised ~ 920 nm continuous wave laser (MSquared SOLSTIS and New Focus Velocity TLB-6700) beams modulated through electro-optical modulators (EOSPACE AZ-0S5-10-PFA-PFA-930 and iXblue NIR-MX950-LN-20-P-P-FA-FA) introduced the optical pumping and spin rotation necessary for the all-optical control. Mounting the modulators on a temperature-stabilised copper plate and periodically calibrating their DC bias input provided an on/off output power extinction ratio of over three orders of magnitudes. This extinction ratio ensured that optical pumping and spin rotation were negligible when the voltage input of the modulator was set to zero. Before and after the application of any rotation pulse sequence (Ramsey or CPMG), we optically pumped the $|\downarrow\rangle \leftrightarrow |\uparrow\downarrow, \downarrow\rangle$ transition and collected fluorescence emitted via the $|\uparrow\downarrow, \downarrow\rangle \rightarrow |\uparrow\rangle$ transition. While such optical pumping initialised the spin in the $|\uparrow\rangle$ state, the emitted fluorescence signal indicated the spin state prior to the pumping pulse (as this fluorescence is only associated with the probability of the $|\downarrow\rangle$ state).

The fluorescence signal was collected from an objective lens with a numerical aperture of 0.68, spectrally filtered through a 0.07 nm full width half maximum Gaussian bandpass filter (WL Photonics WLTF-NE-P-930) and detected on a superconducting nanowire single photon detector (Opus one 950 nm). To optimise the collection signal-to-noise ratio, motorised quarter and half wave-plates rejected the circularly polarised laser light directly reflected from the sample by six orders of magnitude. Finally, three microwave waveforms generated by a 65 Gs/S arbitrary waveform generator (Keysight M8195A) were used to synchronise between the experimental equipment. First, pulses of a harmonic signal with frequency $\frac{\omega_0}{2}$ were injected to one electro-optical modulator to introduce spin rotations. Then, a waveform consisting of square pulses was injected to the second modulator to switch the pumping laser on and off. A final square wave was then used to trigger the time-resolved detector.

Realisation of Pulse Sequences. To realise the Ramsey sequence, we first prepared the quantum dot spin in the $\frac{|\uparrow\rangle+|\downarrow\rangle}{\sqrt{2}}$ state by resonantly pumping the $|\downarrow\rangle \leftrightarrow |\uparrow\downarrow, \downarrow\rangle$ transition to initialise the spin in the $|\uparrow\rangle$ state, followed by a rotation $\frac{\pi}{2}$ -pulse. Then, the spin freely evolved for a given time. Finally, an additional $\frac{\pi}{2}$ -pulse projected the spin state back to either of the ground states $|\uparrow\rangle, |\downarrow\rangle$ (depending on the phase of the $\frac{\pi}{2}$ -pulse, Fig. 1e) and the spin coherence was measured using an optical pumping pulse. Collecting fluorescence while varying the free evolution time resulted in the Ramsey decay function. Separate results involving final projections to the $|\uparrow\rangle$ and $|\downarrow\rangle$ states (as presented in Fig. 1e for the Ramsey sequence applied after the nuclear spin polarisation) were normalised with respect to each other to cancel technical drifts. The result was normalised to

provide a contrast value of 1 for time $t = 0$ (Fig. 1d). The realisation of CPMG sequences (Fig. 2a) was similar to that of the Ramsey sequence, with the additional application of n π -pulses between the first and second $\frac{\pi}{2}$ -pulses. The phase of the π -pulses was shifted by 90° from the phase of the $\frac{\pi}{2}$ -pulses to mitigate potential contrast drop due to fluctuations in the amplitude and phase of the rotation field [12, 31]. The total spin interrogation time was varied to extract the coherence functions depicted in Fig. 2.

Optimisation of Experimental Parameters. The Rabi frequency of spin rotation utilizing Raman control is given by [10, 11, 14, 15] $\Omega_R = \frac{\Omega^2}{\Delta}$ where Ω^2 is linearly proportional to the laser power, P , and Δ is the spectral detuning of the laser from the optical transitions of the quantum dot. Considering the adiabatic elimination principle, $\Delta \gg \Omega$ must be satisfied to avoid the population of the excited states [10, 11, 14, 15]. Maximizing the Rabi frequency Ω_R by increasing the laser power or reducing the detuning would reduce the duration of the π -pulses and provide access to spin dynamics at short timescales, thereby increasing the bandwidth of the noise spectroscopy (Supplementary Note 2). However, the detuning cannot be reduced arbitrarily due to potential population of the excited states, and the laser power cannot be increased arbitrarily due to laser-induced tunnelling that leads to spin relaxation (Supplementary Note 3). As a result, we optimised the parameters for the rotation laser and found $\Delta \approx 535$ GHz (1.5 nm) and $P \approx 15$ μ W for the observation of eight Rabi oscillations at a frequency of $\Omega_R \approx 150$ MHz.

Finally, optimised polarisation of the nuclear ensemble requires simultaneous optical pumping and spin rotation at rates on the order of the Larmor components of the nuclear spins [11]. For a magnetic field of $B = 2.4T$, for example, a rotation laser power of 2 μ W and optical pumping power of 5 nW provided the optimal coherence time result of $T_2^* \approx 48$ ns, presented in Fig. 1d. Considering a $\Gamma_0 \approx 250$ MHz linewidth of the quantum dot excited states, these optical powers translate to a rotation rate of ≈ 20 MHz and a pumping rate of ≈ 27.5

MHz, consistent with previous work [11].

ACKNOWLEDGEMENTS

We thank M. Atatüre, C. Le Gall, D. A. Gangloff, N. Bar-Gill and Y. Romach for fruitful discussions. This work has been supported by the Physics Frontier Center at the Joint Quantum Institute, the National Science Foundation (Grants PHY1415485 and ECCS1508897), and the ARL Center for Distributed Quantum Information (Grant W911NF1520067). D. F. acknowledges support by the Fulbright Postdoctoral Fellowship and the Israel Council for Higher Education Quantum Science and Technology Scholarship. A.S.B. and S.G.C.G. acknowledge support from the U.S Office of Naval Research. R.M.P. acknowledges support through an appointment to the Intelligence Community Postdoctoral Research Fellowship Program at the University of Maryland, administered by Oak Ridge Institute for Science and Education through an interagency agreement between the U.S. Department of Energy and the Office of the Director of National Intelligence.

AUTHOR CONTRIBUTIONS

D.F. and E.W. conceived and designed the experiment. D.F. and H.S. performed measurements. D.F. and Z.L. constructed the experimental setup. D.F. analysed experimental results, performed simulations, and wrote the manuscript. A.S.B. and S.G.C. provided the sample grown by molecular beam epitaxy. All authors contributed to scientific discussions and the preparation of the manuscript.

COMPETING INTERESTS

The authors declare no competing interests.